20$^{th}$ EAWE PhD Seminar on Wind Energy
24-26 September 2024
Visby, Sweden

# Study of the three-dimensional coherent structures in the wake of flatback airfoils

**Konstantinos Kellaris**[a], **George Papadakis**[b], and **Marinos Manolesos**[a]

[a]School of Mechanical Engineering, National Technical University of Athens
[b]School of Naval Architecture and Marine Engineering, National Technical University of Athens

Email: kkellaris@mail.ntua.gr

*Keywords*: flatback airfoils, low-drag regime, secondary wake instabilities, DES, modal analysis

## 1 Introduction

As wind turbine (WT) rotor diameters increase, aiming to lower the Levelized Cost of Energy (LCOE), flatback (FB) airfoils, i.e., airfoils with a blunt trailing edge (TE), have gained traction recently. FB airfoils are placed at the root of WT blades, providing various aerodynamic, structural, and aeroelastic benefits. From an aerodynamics point of view, FB airfoils can provide higher lift values due to the reduced adverse pressure gradient over the aft part of the suction side [1]. In addition, their aerodynamic performance is insensitive to surface roughness compared to traditional sharp TE airfoils [1]. Early studies indicated that blades with flatpack airfoils can be up to 16% lighter than blades that use traditional airfoils without inducing any performance penalty [2]. Additionally, due to the blunt TE and increased blade cross-sectional area, FB blades have increased flapwise stiffness. However, FB airfoils come with an increase in drag force and noise [1, 3]. Consequently, several TE flow control devices have been proposed to improve their aerodynamic performance and decrease the associated drag penalty [3, 4, 5].

Most of the studies regarding FB airfoils have focused either on their aerodynamic/aeroacoustic performance [3, 6] or the wake characteristics of their flow [7, 5, 8] at $a = 0^{\circ}$, or relatively low angles of attack (AoA). Recently, studies were performed up to near-stall or post-stall [9, 10] AoA to provide new insights regarding the three-dimensional wake behaviour using high-fidelity tools. In experiments [11, 12, 13, 3, 4] and in simulations [14, 3, 9], a low-drag "pocket" arises in a region of AoA before stall, however, no one has yet sufficiently explained it.

## 2 Methods

### 2.1 Computational Fluid Dynamics

The present investigation focused on the LI30-FB10 airfoil, i.e., an airfoil with a maximum thickness of $0.3c$ and a trailing edge height of $h_{TE} = 0.106c$, where $c$ is the chord length, also investigated in [4, 5, 9]. High-fidelity simulations were performed with the in-house solver MaPFlow [15] to solve the three-dimensional incompressible unsteady Navier-Stokes equations using the artificial compressibility method [16] and the Finite Volume discretization. An O-type grid spanning 50 chord lengths with approximately 10 million cells was used following previous computational studies [5, 9]. The grid had a spanwise length of one chord, while the non-dimensional distance of the first cell from the airfoil was $y^{+} = 0.1$. The airfoil was investigated at a high Reynolds number, namely $Re = 1.5 \times 10^{6}$, using the IDDES method [17]. This hybrid turbulence modelling approach blends the Spalart-Almaras RANS model with the Smagorinsky LES model. Specifically, the RANS variant of the model is employed near the airfoil, while the LES variant is employed away from the airfoil. The necessary grid layers and refinement around the airfoil (RANS region) are shown in Figure 1(a), while Figure 1(b) demonstrates the low-drag pocket discussed in the previous section.

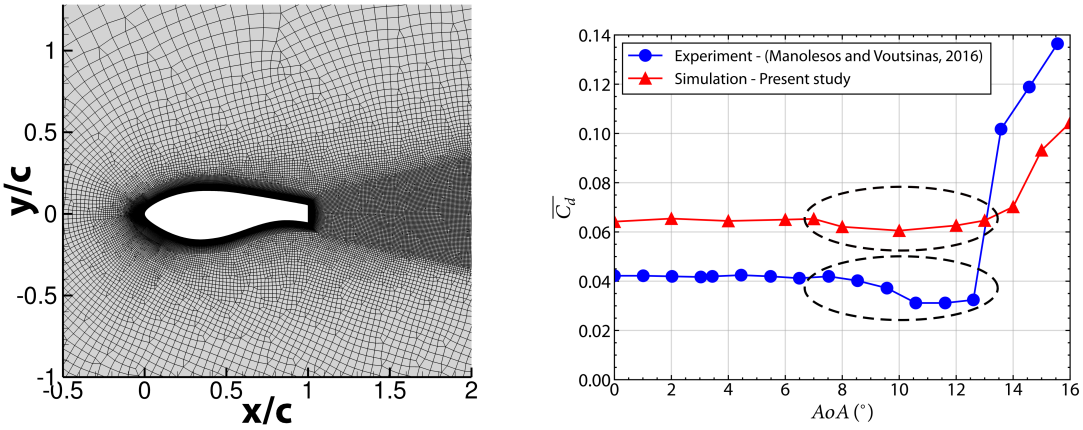


(a) (b)

Figure 1: (a): Detail of the grid refinement layers around the LI30-FB10 airfoil. (b): The variation of the drag coefficient $C_d$ with the angle of attack and the low-drag regime is denoted with dashed ellipses.

### 2.2 Modal Analysis of Wake Structures

In order to extract the three-dimensional wake coherent structures/modes, the multiscale Proper Orthogonal Decomposition (mPOD) method [18] was utilized for two angles of attack—one inside $(12^\circ)$ and one outside $(0^\circ)$ of the low-drag pocket. At each simulation timestep, the grid data are interpolated onto a Cartesian grid spanning one chord length at the streamwise and spanwise directions and half chord length at the $y$-normal direction. Afterward, the dataset is organized into a large matrix where each column represents a timestep and each row a point in time. Then, by applying suitable band-pass filters to the temporal correlation matrix and performing POD for each filtered scale, mPOD yields a representation of the dataset modes that retain the energy optimality of the POD while simultaneously presenting more pure spectral content compared to the plain POD. For visualization purposes, we utilize Q-criterion [19] isosurfaces of the spatial coefficients of each mode coloured by either streamwise or spanwise vorticity. Finally, we extract the dominant frequency of each mode from the spectral behaviour of the temporal coefficients of each mode.

## 3 Results

The vortical structures found in the two cases are shown in the left panels of Figure 2 using Q-criterion isosurfaces coloured with spanwise vorticity. Firstly, the Bénard-von Kármán (primary) instability is evident for both cases. Additionally, the secondary instabilities, i.e. pairs of counterrotating vortices in the streamwise direction that connect two consecutive primary spanwise vortices (white Q-criterion isosurfaces) are also shown in Figure 2. The wake is more organized for the low-drag $(12^\circ)$ case, and the structure of the secondary instability observed in both cases is more apparent compared to the high-drag $(0^\circ)$ case.

The primary instability dominates the first (most energetic) mPOD modes and is omitted from this abstract in the interest of brevity. Specifically, the primary instability and its harmonics appear throughout the first 10 and 6 modes for the $(0^\circ)$ and $(12^\circ)$ cases, respectively.

As shown in the right panels of Figure 2, the first modes that exhibit dominant spanwise behaviour are the 11th and 7th modes for the high-drag $(0^\circ)$ and low-drag $(12^\circ)$ cases, respectively. At $(0^\circ)$ the associated Strouhal number $(St = 0.018)$ is an order of magnitude smaller than the one at the $(12^\circ)$ case $(St = 0.106)$. In addition, the vortical pairs appear to be distorted along the span, an effect that is possibly introduced by the oblique shedding of the primary instability. We estimate the spanwise wavelength of the secondary instabilities, counting the number of vortex pairs along the span, leading to a spanwise wavelength of approximately $\lambda_z = 1h_{TE}$ and $\lambda_z = 1.4h_{TE}$ at $(0^\circ)$ and $(12^\circ)$, respectively.

Finally, while a comprehensive framework exists for characterizing the secondary instabilities in the wake of cylindrical bluff bodies, this is not the case for elongated bluff bodies. The characterization of the secondary

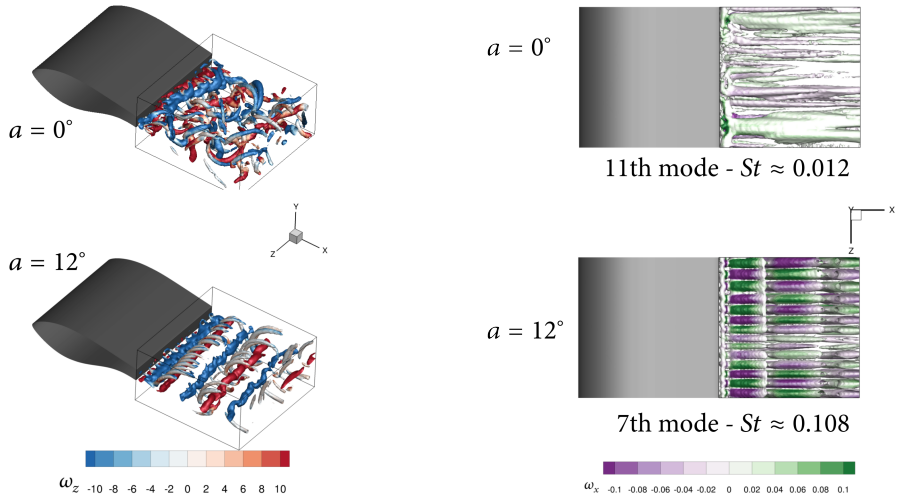


Figure 2: Q-isosurfaces coloured with vorticity. Left: Indicative snapshots for the high-drag $(0^\circ)$ (top) and the low-drag $(12^\circ)$ (bottom) cases coloured with spanwise vorticity. Right: The first mPOD modes exhibiting dominant spanwise behaviour at $(0^\circ)$ (top) and $(12^\circ)$ (bottom) coloured with streamwise vorticity.

instability at $(0^\circ)$ does not correspond to a previously identified coherent mode, as the oblique shedding and the vortex dislocations significantly affect the topology of the wake. On the other hand, at $(12^\circ)$, the modes have a frequency that is a subharmonic of the primary instability. In addition, as shown in the bottom right panel of Figure 2, the streamwise vortical pairs' rotation direction changes at each primary vortex-shedding cycle. Therefore, the instability is characterized as the Mode S′ identified by [20].

# 4 Conclusions

In summary, the three-dimensional coherent structures for the flow past a flatback airfoil were investigated for two angles of attack—one inside $(12^\circ)$ and one outside $(0^\circ)$ of the low-drag pocket. Namely, the primary instability (Bénard-von Kármán vortex street) dominates the wake for the most energetic modes in both cases. However, the wake is more organized at the $(12^\circ)$ case. The first modes demonstrating spanwise behaviour for the high-drag $(0^\circ)$ and the low-drag $(12^\circ)$ cases are the 11th and 7th modes, respectively. However, the behaviour identified in these modes differs significantly for both cases. In the low-drag case $(0^\circ)$, the instability corresponds to the mode S′ described for the flow past elongated bluff bodies [20], while the instability at the high-drag $(0^\circ)$ case cannot be characterized under a pre-existing framework. These new insights about the wake behaviour and organization, in combination with the existence of the low-drag pocket, can potentially be used to formulate a passive drag reduction strategy based on spanwise excitation using the wavelength identified for the Mode S′ instability.

# Acknowledgements

The authors kindly acknowledge the financial support of the European project 'TWEET-IE' funded by the European Union's Horizon 2020 Research and Innovation Programme (Grant Agreement 101079125). K. Kellaris acknowledges the support by the Hellenic Foundation for Research and Innovation (HFRI) under the 5th Call for HFRI PhD Fellowships (Fellowship Number: 20455). Additionally, this work was supported by computational time granted from the National Infrastructures for Research and Technology S.A. (GRNET S.A.) in the National HPC facility - ARIS - under project 'HPC4FAIR' with ID pr014018_thin.

# References

[1] J. P. Baker, E. A. Mayda, and C. P. Van Dam. Experimental analysis of thick blunt trailing-edge wind turbine airfoils. *Journal of Solar Energy Engineering*, 128(4):422–431, Nov. 2006.

[2] D. Griffith and P. Richards. The SNL100-03 Blade: Design Studies with Flatback Airfoils for the Sandia 100-meter Blade. Technical Report SAND2014-18129, 1159116, 537751, Sandia National Lab, Albuquerque, NM (United States), Sept. 2014.

[3] M. F. Barone, D. E. Berg, W. J. Devenport, and R. A. Burdisso. Aerodynamic and aeroacoustic tests of a flatback version of the DU97-W-300 airfoil. Technical Report SAND–2009-4185, 1504612, Aug. 2009.

[4] M. Manolesos and S. G. Voutsinas. Experimental study of drag-reduction devices on a flatback airfoil. *AIAA Journal*, 54(11):3382–3396, Nov. 2016.

[5] G. Papadakis and M. Manolesos. The flow past a flatback airfoil with flow control devices: Benchmarking numerical simulations against wind tunnel data. *Wind Energy Science*, 5(3):911–927, July 2020.

[6] M. Fuchs, P. Weihing, T. Kuehn, M. Herr, A. Suryadi, C. Mockett, H. Knobbe-Eschen, F. Kramer, and T. Knacke. Two computational studies of a flatback airfoil using non-zonal and embedded scale-resolving turbulence modelling approaches. In *28th AIAA/CEAS Aeroacoustics 2022 Conference*, Southampton, UK, June 2022. American Institute of Aeronautics and Astronautics.

[7] G. Wang, L. Zhang, and W. Z. Shen. LES simulation and experimental validation of the unsteady aerodynamics of blunt wind turbine airfoils. *Energy*, 158:911–923, Sept. 2018.

[8] L. Hongpeng, W. Yu, Y. Rujing, X. Peng, and W. Qing. Influence of the modification of asymmetric trailing-edge thickness on the aerodynamic performance of a wind turbine airfoil. *Renewable Energy*, 147:1623–1631, Mar. 2020.

[9] M. Manolesos and G. Papadakis. Investigation of the three-dimensional flow past a flatback wind turbine airfoil at high angles of attack. *Physics of Fluids*, 33(8):085106, Aug. 2021.

[10] G. Bangga, F. Seel, T. Lutz, and T. Kühn. Aerodynamic and acoustic simulations of thick flatback airfoils employing high order DES methods. *Advanced Theory and Simulations*, 5(8):2200129, May 2022.

[11] H. A. Smith and R. F. Schaefer. Aerodynamic characteristics at reynolds numbers of 3.0 x 10 (exp 6) and 6.0 x 10 (exp 6) of three airfoil sections formed by cutting off various amounts from the rear portion of the NACA 0012 airfoil section. Technical report, 1950.

[12] M. Post, R. Jones, A. Denton, and R. Millard. Characterization of a flatback airfoil for use in wind power generation. In *46th AIAA Aerospace Sciences Meeting and Exhibit*, page 1330, 2008.

[13] J. Baker and C. P. van Dam. Drag reduction of blunt trailing-edge airfoils. In *BBAA VI International Colloquium on: Bluff Bodies Aerodynamics & Applications*, Milano, Aug. 2008.

[14] T. Winnemöller and C. P. Van Dam. Design and Numerical Optimization of Thick Airfoils Including Blunt Trailing Edges. *Journal of Aircraft*, 44(1):232–240, Jan. 2007.

[15] G. Papadakis. *Development of a Hybrid Compressible Vortex Particle Method and Application to External Problems Including Helicopter Flows*. PhD thesis, National Technical University of Athens, 2014.

[16] D. Ntouras and G. Papadakis. A coupled artificial compressibility method for free surface flows. *Journal of Marine Science and Engineering*, 8(8):590, Aug. 2020.

[17] P. R. Spalart, S. Deck, M. L. Shur, K. D. Squires, M. Kh. Strelets, and A. Travin. A New Version of Detached-eddy Simulation, Resistant to Ambiguous Grid Densities. *Theoretical and Computational Fluid Dynamics*, 20(3):181–195, July 2006.

[18] M. A. Mendez, M. Balabane, and J.-M. Buchlin. Multi-scale proper orthogonal decomposition of complex fluid flows. *Journal of Fluid Mechanics*, 870:988–1036, May 2019.

[19] J. C. R. Hunt, A. A. Wray, and P. Moin. Eddies, streams, and convergence zones in turbulent flows. Dec. 1988.

[20] K. Ryan, M. C. Thompson, and K. Hourigan. Three-dimensional transition in the wake of bluff elongated cylinders. *Journal of Fluid Mechanics*, 538(-1):1, Aug. 2005.